*Int. J. Electrochem. Sci.*, 7 **(2012)** 3717 - 3725

International Journal of
ELECTROCHEMICAL
SCIENCE
www.electrochemsci.org

# Potentiostatic Electrosynthesis and Characterization of Triazinethiolsilane Nanofilm on Aluminum Alloy

*Fang Wang*[*], *Yanni Li, Yuefei Li, Haining Zhang*

College of Science, Northwest Agriculture & Forest University, No.22, XiNong Road, Shaanxi-Yangling, 712100, China
[*]E-mail: wangfang4070@nwsuaf.edu.cn

*Received:* 12 February 2012 / *Accepted:* 13 March 2012 / *Published:* 1 April 2012

Poly(6-(3-triethoxysilylpropyl)amino-1,3,5-triazine-2,4-dithiol) nanofilm (PTESPA) was prepared by the potentiostat of 6-(3-triethoxysilylpropyl)amino-1,3,5-triazine-2,4-dithiol monosodium (TESPA) on aluminum alloy surface. The polymeric nanofilm was characterized by means of Fourier transform infrared spectroscopy (FT-IR), x-ray photoelectron spectroscopy (XPS) and cyclic voltammetry test. The morphologies of the polymeric nanofilm were observed by scanning electron microscope (SEM) and atomic force microscopy (AFM). FT-IR spectra showed that PTESPA film was obtained on aluminum alloy surface by the potentiostat. The results of XPS and cyclic voltammetry test indicated that the optimal potential for potentiostatic electrosynthesis of triazinethiolsilane was 7V. The results of SEM and AFM indicated that the polymeric nanofilm prepared at 7V was the most compact and homogenous.

**Keywords:** Aluminum Alloy; Polymeric nanofilm; Potentiostat; Electrosynthesis

## 1. INTRODUCTION

Aluminum alloys have been widely used in numerous industrial fields (e.g. aerospace industry) for the low density, easy modeling and high mechanical intensity [1, 2]. However, they are inclined to be corroded under severe conditions. The researchers had adopted many different procedures to improve their corrosion resistance. Among them, organic coatings applied to metal surfaces provided corrosion protection by introducing a barrier to water and oxygen permeability, ionic transport and electrical conduction, which is highly recommended to be applied to replace the traditional chromating as an environmental friendly method [3-5]. Triazinedithiols (TDTs) organic coatings have been received increasing attention in recent years and applied in many fields [6-8] (e.g. metal protection) for

the high reactivity and functionality. Meanwhile, the techniques for preparing TDTs polymeric nanofilm developed substantially. Electrodeposition technique was mainly used to fabricate TDTs functional nanofilm in recent years, including cyclic voltammetry [9] or galvanostatic [10] methods. These two electrochemical methods had already been studied systematically. However, the polymeric nanofilm obtained by the techniques was thin or time-consuming, which makes its application in wider fields limited. Therefore, it is necessary to find new technique to fabricate ideal thicker and denser triazinedithiol polymeric nanofilm.

Potentiostatic electrodeposition technique has been utilized to prepare functional film on metal surface in recent years as an emerging technique for its high reproducibility, time-saving, low cost, etc [11]. However, the systematical researches on potentiostatic method for preparing TDTs polymeric film have not been reported as much [12-14]. In this study, we focused on potentiostatic method to fabricate such functional polymeric nanofilm, and investigated the optimal potential for homogeneous and packed polymeric nanofilm preparation of triazinethiolsilane on aluminum alloy surface.

## 2. EXPERIMENTAL SECTION

### *2.1. Materials*

Aluminum alloy-AA5052 (Cu: 0.1%, Si: 0.2%, Fe: 0.4%, Mn: 0.1%, Mg: 2.8%, Zn: 0.1%, Cr: 0.3%, others: 0.15%) test samples (50 × 30 × 0.3mm) were prepared by cutting a large plate into pieces. All test samples were degreased by ultrasonic washing in acetone for 15min, and dried in nitrogen air. 6-(3-triethoxysilylpropyl)amino-1,3,5-triazine-2,4-dithiol monosodium (TESPA) (Figure 1) was synthesized according to the method described in the previous study [15]. All of the chemicals were employed as analytical reagent (AR) without further purification. Distilled water was used as solvent and sodium nitrite ($NaNO_2$) was applied as supporting electrolyte. The concentrations of TESPA and $NaNO_2$ were kept at 3mM and 0.15M, respectively.

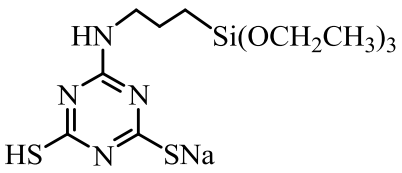


**Figure 1.** Structure of TESPA

### *2.2. Preparation of polymeric nanofilm (PTESPA)*

The potentiostatic electrosynthesis of TESPA was performed using an electrochemical workstation (CHI 660C). The electrolytic cell was equipped with a working electrode (aluminum plates, WE), two counter electrodes (stainless steel plates, CE) and a reference electrode (saturated calomel electrode, SCE), then filled with electrolytic solution containing TESPA in distilled water. All

given potentials were referenced to the SCE. The potentiostat was carried out from 2V to 8V for 30s at 10°C without stirring. After the electrosynthesis, the working electrode was removed from the electrolytic cell and immediately rinsed by distilled water and ethanol, then dried in air.

### *2.3. Characterization*

FT-IR was carried out by attenuated total reflection spectroscopy (Bruker Tensor 37). XPS was performed to determine the elemental composition of PTESPA naofilm on AA5052 surface. The spectra were obtained by using ULVAC PHI-5600 spectrometer equipped with monochrome Al Kα radiation (1,486.6eV). The pressure in the preparation chamber was less than $10^{-7}$ Torr and less than 4 $\times$ $10^{-10}$ Torr in the analysis chamber. The photoelectron spectra were recorded with a take-off angle of 45°. The compactness of the polymeric nanofilms was studied by cyclic voltammetry from -0.6V to 2V at a scanning rate of 10mV/s in 0.1% $H_2SO_4$ solution with two stainless steel plates as counter electrode. The morphologies of the PTESPA naofilm covered surface were also observed by SEM (JSM-6360LV) at an accelerating voltage of 20kV and AFM (MULTIMODE V, VEECO INSTRUMENTS INC) by contact mode.

## 3. RESULTS AND DISSUSION

### *3.1. FT-IR spectra analysis*

Figure 2 shows FT-IR spectra of PTESPA nanofilm obtained by potentiostat on AA5052 plate. In the FT-IR spectra, the presence of triazine ring is confirmed by absorption peaks at 1,478, 1,527 and 1,541 $cm^{-1}$ due to >C=N- bonds.

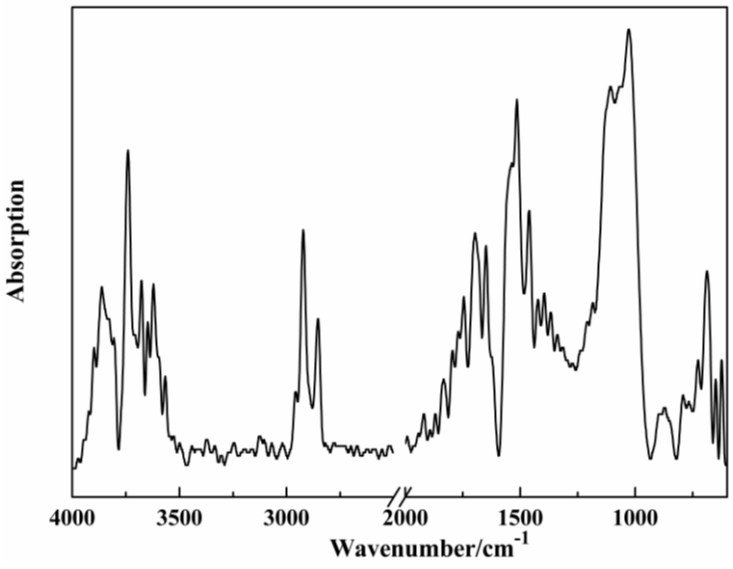


**Figure 2.** FT-IR spectra of PTESPA nanofilm on AA5052 surface

Triethoxysilylpropyl amino groups are confirmed by absorption peaks at 2,765 and 2,839 $cm^{-1}$ due to C-H symmetric stretching vibrations of $CH_3$- and -$CH_2$- as well as by absorption peaks at 2,946 $cm^{-1}$ due to C-H asymmetric stretching vibrations of $CH_3$- and -$CH_2$-. Also the absorption peak at 1123 and 1028 $cm^{-1}$ were due to the Si-O-Si stretching, indicating that the condensation reaction of triethoxysilylpropyl amino groups occurred to obtain the -Si-O-Si- network structure. The appearance of adsorption bands in the 3600-3900 $cm^{-1}$ regions is assigned to hydrogen bond of hydroxyl groups (-OH) [15]. It was suggested that non-condensed silanol groups were existed in the outside part of PTESPA film on AA5052 surface. The weak peak at 884 $cm^{-1}$ suggested the -C-S stretching vibration. The weak peak at 948 $cm^{-1}$ was also observed due to the alumina. It was indicated that the electrosynthesis of TESPA and oxidative reaction of aluminum occurred simultaneously. These results showed that the PTESPA nanofilm was obtained on AA5052 surface.

### *3.2. Effect of the potential on polymeric nanofilm*

Figure 3 shows the potentiostat curves for fabrication of PTESPA nanofilm at different potentials. It is noted that the potential has no significant influence on the general shape of the curves. From the curves at the position of 2.5s, it can be seen that the reaction current gradually increases as the potential is improved. It was suggested that the oxidative current was proportional to the concentration gradient at the interface of AA5052. At the low potentials, TESPA can produce relevant radicals by releasing an electron to the anode, which decreases the concentration of TESPA on AA5052 surface. Also, as the current is limited to the diffusion rate of TESPA monomer, it is correspondingly low under low potentials.

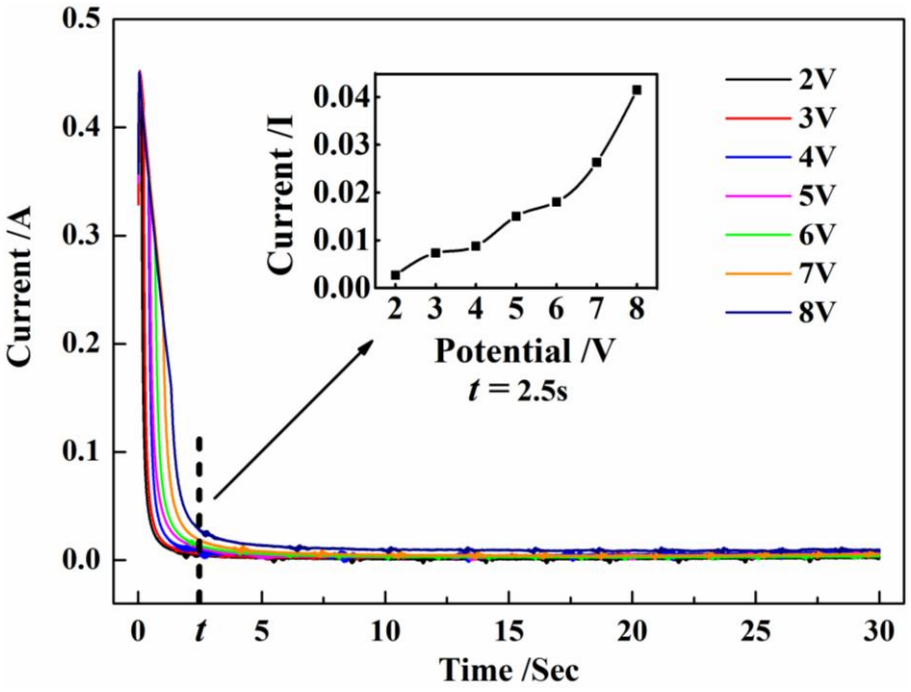


**Figure 3.** Potentiostat curves for fabrication of PTESPA film at different potentials

Therefore, the potential was not high enough for improving the diffusion rate of TESPA to reach almost zero concentration on AA5052 surface, and the current efficiency is not high, neither. At the high potentials, although the concentration of TESPA on AA5052 surface can hardly reach zero, the diffusion rate of TESPA is greatly promoted, which makes the concentration gradient on AA5052 surface much higher. So the current efficiency is high and the formation of PTESPA at high potentials is better than that at low potentials.

### *3.3. XPS analysis*

The PTESPA nanofilm at different potentials was investigated by XPS (Figure 4). The peaks corresponding to oxygen (O1s), nitrogen (N1s), carbon (C1s), sulfur (S2p), silicon (Si2p) and aluminum (Al2p) were analyzed [6]. The peaks of O1s (532.0 eV), C1s (284.8 eV) and Al2p (73.8 eV) could be observed obviously at 2V and 3V, while the peak intensities of N1s (398.9 eV), S2p (164.1 eV) and Si2p (101.8 eV) were very weak. It was suggested that the PTESPA nanofilm at low potentials was thinner. In the case of electrosynthesis from 4V to 7V, an increased amount of N (N1s), S (S2p) and Si (Si2p) and decreased amount of O (O1s) and Al (Al2p) could be detected on AA5052 surface. While a decreased amount of N (N1s), S (S2p) and Si (Si2p) and increased amount of O (O1s) and Al (Al2p) was detected at the potential of 8V. It was suggested that the polymeric nanofilm was broken down to some extent at the potential of 8V. Hence, the potentials exceeded 8V were not chosen.

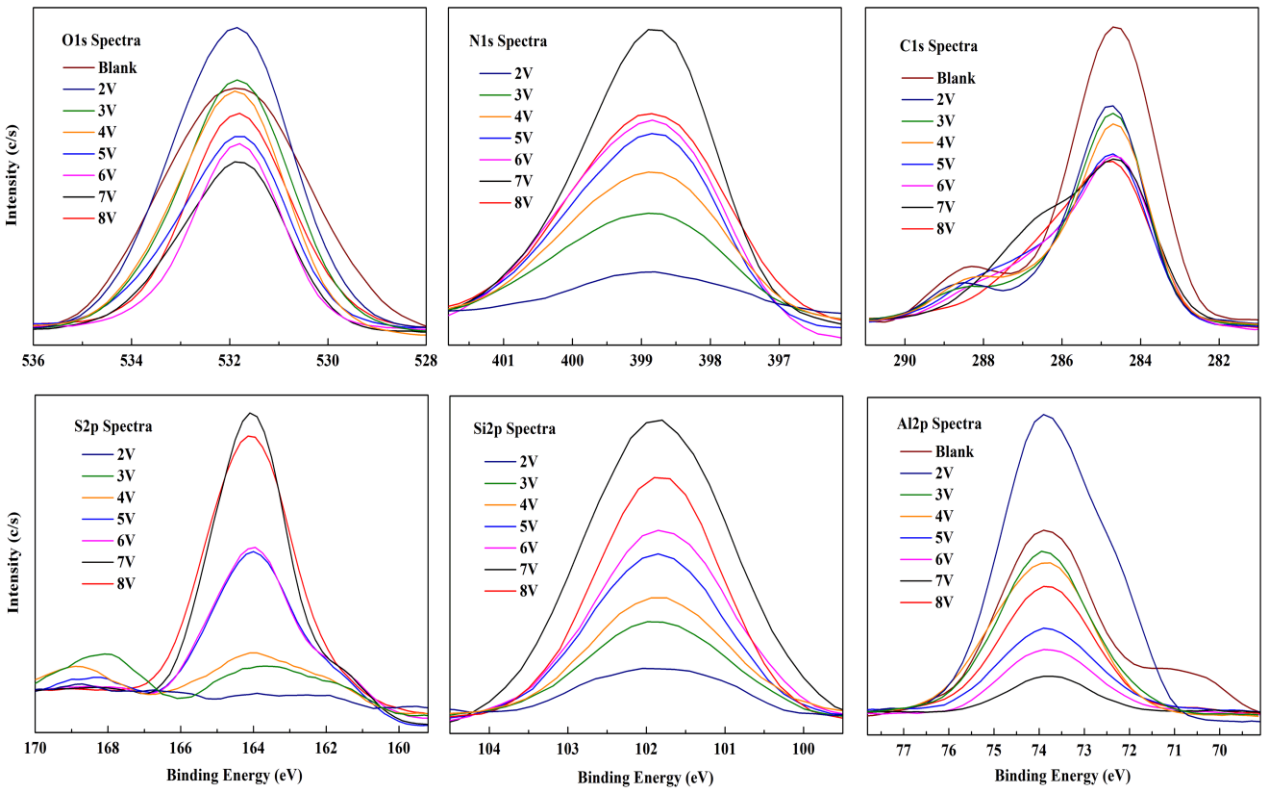


**Figure 4.** XPS spectra of PTESPA film at different potentials

Table 1 shows the atomic concentrations of PTESPA nanofilm electrosynthesized at different potentials. It can be seen that the atomic concentrations of Si2p, N1s and S2p increase, while that of Al2p and O1s decrease on AA5052 surface at the higher potentials. It was indicated the continuous formation of polymeric nanofilm at the higher potential, and the concentrations of Si2p, N1s and S2p reached the highest at the potential of 7V. The results showed that the optimal potential for PTESPA nanofilm electrosynthesis was 7V.

**Table 1.** Atomic concentration (%) of PTESPA nanofilm at different potentials

| Potential(V) | O1s (%) | N1s (%) | C1s (%) | S2p (%) | Si2p (%) | Al2p (%) |
|---|---|---|---|---|---|---|
| Blank | 30.7 | \ | 62.9 | \ | \ | 1.9 |
| 2.0V 30s | 20.4 | 1.5 | 25.7 | 0.5 | <0.1 | 8.6 |
| 3.0V 30s | 18.3 | 3.6 | 29.3 | 0.9 | 0.3 | 4.6 |
| 4.0V 30s | 17.7 | 6.1 | 29.8 | 1 | 1.7 | 4.4 |
| 5.0V 30s | 13.7 | 8.1 | 32.7 | 2.0 | 1.7 | 2.8 |
| 6.0V 30s | 13.1 | 8.4 | 29.3 | 2.0 | 1.9 | 2.4 |
| 7.0V 30s | 11.1 | 9.5 | 30.6 | 3.3 | 3.2 | 1.1 |
| 8.0V 30s | 15.6 | 7.0 | 25.8 | 1.4 | 2.0 | 3.4 |

### *3.4. SAM and AFM results*

Based on the results of FT-IR and XPS spectra, the surface morphologies of blank and PTESPA nanofilm covered AA5052 were also observed by SEM (Figure 5). It can be seen that the scratches with the rolling process could be clearly observed on the blank AA5052. Fine intermetallic particles which are aligned along the rolling direction can be seen, distributing all over the surface. With the potential increasing, the original morphologies compared with that of PTESPA nanofilm covered AA5052 surface become more invisible. Some pores and comparatively large fine intermetallic particles could still be observed for low potentials while they could hardly be seen at the potential of 7V. However, some pores appeared at the potential of 8V. It was deduced that the potentiostatic electrosynthesis was promoted as the potential increased to 7V, and the polymeric nanofilm became denser with the same electrosynthesis time. Also, the surface became more homogenous, compact with higher film coverage. However, the depolymerization reaction of PATESA nanofilm was expected to occur at the potential of 8V, which was found to be deleterious to the coated system behavior. The results are consistent with the conclusion of FT-IR and XPS.

To better understand the surface structure, two and three dimensional micro-structures were observed by AFM (Figure 6 (A) and (B)). It can be seen that the AA5052 surfaces were covered by PTESPA nanofilm compared to the blank. The fringes of AA5052 surface disappeared due to the formation of polymeric nanofilm from 2V to 8V, and the coverage of AA5052 surface became higher. Numerous low mountains and hillocks are observed, indicating that the film is compact to some extent. The data of surface roughness are also listed in the figure 6 (A), which indicate that the nanofilm coverage on aluminum surface becomes higher with potential increasing and the PTESPA nanofilm

obtained at 7V is much thicker. However, when the potential was over 7V, the degree of roughness became lower due to the more rapid formation of polymeric nanofilm and also the depolymerization of PTESPA nanofilm happened. All of the results demonstrated the continuous formation of polymeric nanofilm on AA5052 surface at higher potential, and confirmed that the optimal potential was 7V.

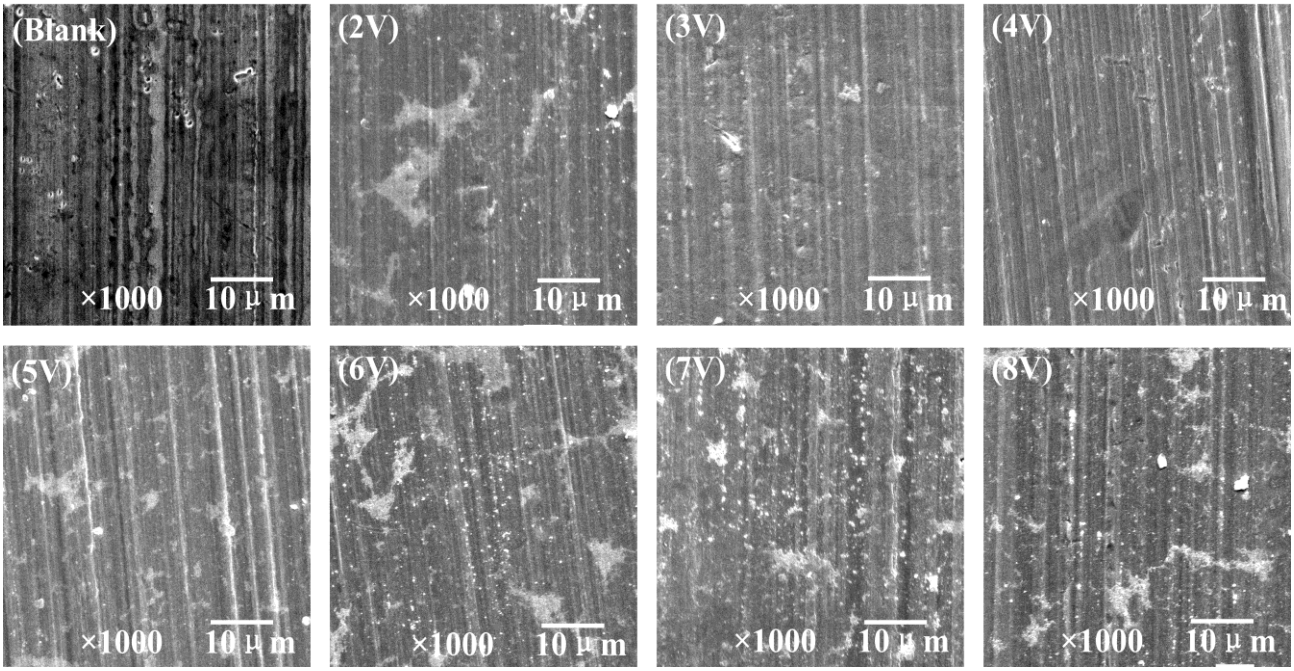


**Figure 5.** SEM images of AA5052 surface covered by PTESPA nanofilm at different potentials

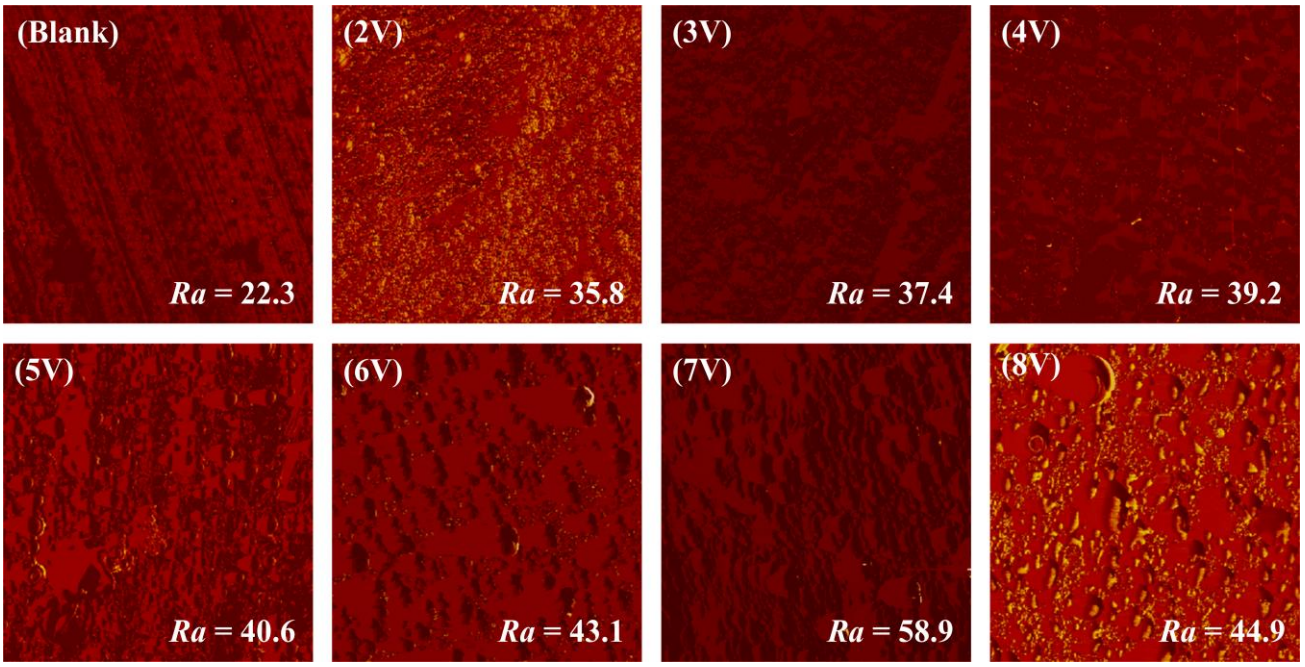


**A**

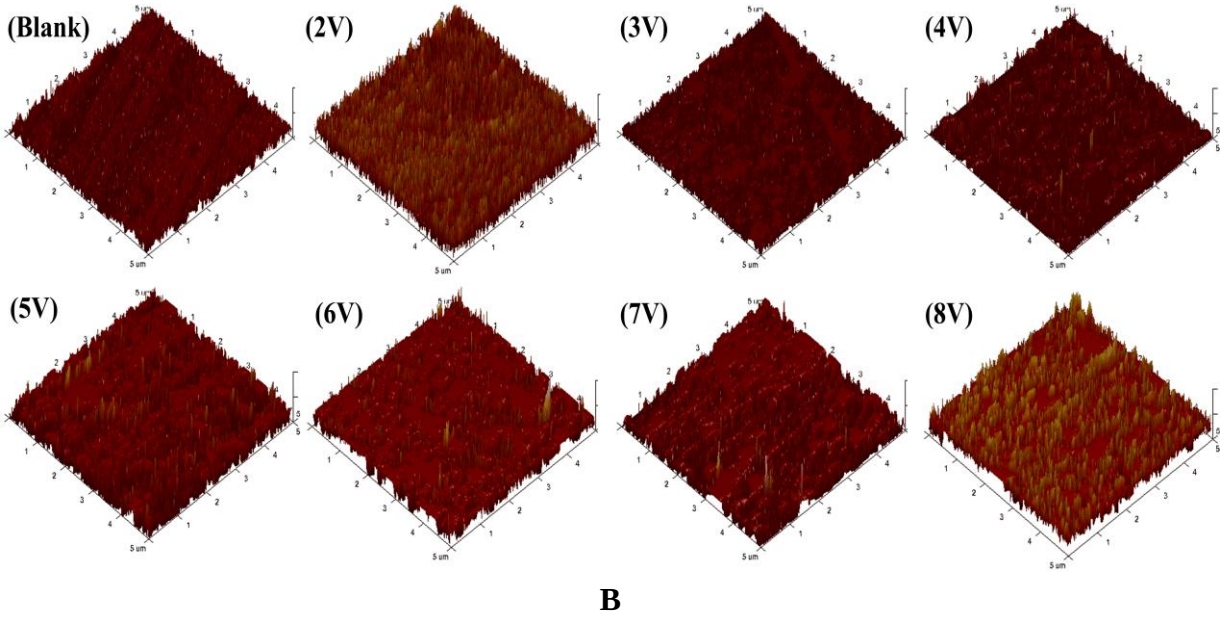


**Figure 6**. AFM images of AA5052 surface covered by PTESPA nanofilm at different potentials. A) 2D images; B) 3D images

### *3.5. Compactness test by cyclic voltammetry*

The cyclic voltammetry curves of the PTESPA nanofilm at different potentials are shown in Figure 7. It is noted that the potential has no significant effect on the general shape of the cyclic voltammogram.

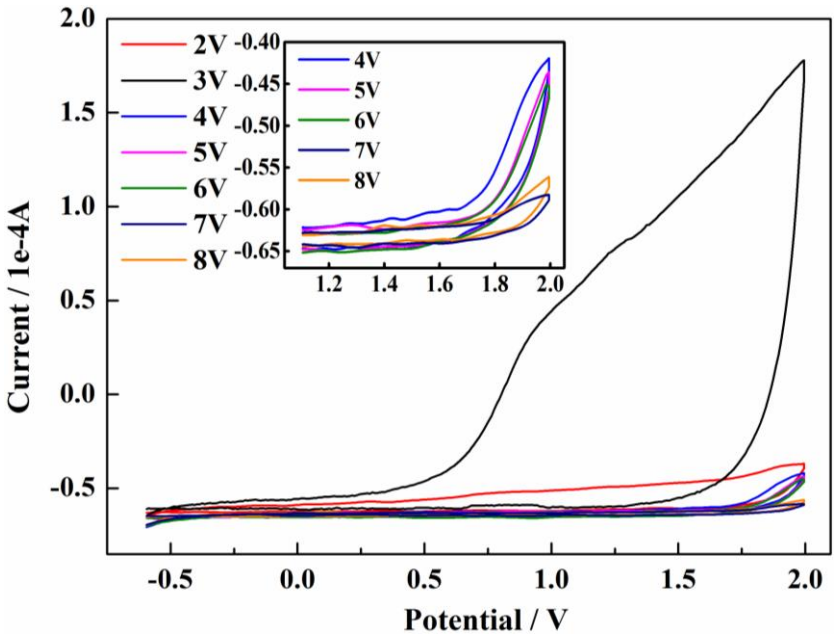


**Figure 7.** Cyclic voltammogram of the PTESPA nanofilm covered AA5052 surface at different potential

The anodic peak at the potential of 2V could be attributed to continuous formation of alumina as a result of electro-oxidation of the AA5052 substrate. And there is no reduction peak of AA5052 oxidized species, which indicates the PTESPA nanofilm or alumina is passivative. The area of cyclic voltammogram significantly decreased at higher potentials, which indicated the formation of PTESPA nanofilm on the AA5052 surface [16]. The reaction currents of the PTESPA nanofilm covered surface largely reduce as the potential increases and was the lowest at the potential of 7V, suggesting the better performance in the protection of the AA5052 surface from oxidation.

## 4. CONCLUSIONS

The PTESPA nanofilm was successfully electrosynthesized by potentiostatic method on AA5052 surface with the confirmation of FT-IR. From the results of XPS, SEM, AFM and compactness test, the optimum value for the electrosynthesis potential was 7V. More uniform and denser PTESPA nanofilm was obtained at the condition of 7V. It is expected that this technique will provide a novel approch for metal surface modification with triazinedithiolsilane.

ACKNOWLEDGEMENTS
The authors gratefully acknowledge Scientific Research Foundation for the Returned Overseas Chinese Scholars, State Education Ministry (No.K314020902) and the Fundamental Research Funds for the Central Universities (No.Z109021008).

## References

1. D. Zhu, W.J.v. Ooij. *Electrochim. Acta* 49 (2004) 1113.
2. P.C.R. Varma, J. Colreavy, J. Cassidy, M. Oubaha, C. McDonagh, B. Duffy. *Thin Solid Films* 518 (2010) 5753.
3. J. Bajat, I. Milosev, Z. Jovanovic, R. Jancic-Heinemann, M. Dimitrijevic, V. Miskovic-Stankovic. *Corros. Sci.* 52 (2010) 1060.
4. F. Zucchi, A. Frignani, V. Grassi, A. Balbo, G. Trabanelli. *Mater. Chem. Phys.* 110 (2008) 263.
5. J. Gray, B. Luan, *J Alloy Compd*, 336 (2002) 88.
6. F. Wang, Y. Li, Q. Wang, Y. Wang. *Int. J. Electrochem. Sci.* 6 (2011) 113.
7. Z. Kang, X. Lai, J. Sang, Y. Li. *Thin Solid Films* 520 (2011) 800.
8. Z. Kang, K. Nakata, Y. Li, *Surface and Coatings Technology*, 201 (2007) 4999.
9. Y. Li, D. Wang, H. Zhang, F. Wang, *Int. J. Electrochem. Sci.* 6 (2011) 4404.
10. Z. Kang, Q. Ye, J. Sang, Y. Li. *J. Mater. Process. Tech.* 209 (2009) 4543.
11. K. Mori, Y. Sasaki, H. Hirahara, Y. Oishi *J. Appl. Polym. Sci.* 82 (2001) 2300.
12. F. Wang, Y. Wang, Y. Li, H. Zhang. J. Wang, *Int. J. Electrochem. Sci.* 6 (2011) 1127.
13. F. Wang, Y. Wang, Y. Li. *Int. J. Mol. Sci.* 11 (2010) 4715.
14. F. Wang, Y. Wang, Y. Li, Q. Wang. *Appl. Surf. Sci.* 257 (2010) 2423.
15. F. Wang, Y. Li, Y. Wang, Z. Cao. *Nanoscale Res. Lett.* 6 (2011) 483.
16. N.C.T. Martins, T. Moura e Silva. M.F. Montemor, J.C.S. Fernandes, M.G.S. Ferreira. *Electrochim. Acta* 55 (2010) 3580.